JMB

Available online at www.sciencedirect.com

ScienceDirect

ELSEVIER

Towards Multiparametric Fluorescent Imaging of Amyloid Formation: Studies of a YFP Model of α-Synuclein Aggregation

Tjakko J. van Ham[1], Alessandro Esposito[2], Janet R. Kumita[3], Shang-Te D. Hsu[3], Gabriele S. Kaminski Schierle[2], Clemens F. Kaminski[2], Christopher M. Dobson[3], Ellen A. A. Nollen[1]* and Carlos W. Bertoncini[3]*

[1]*Department of Genetics, University of Groningen, Groningen, The Netherlands*

[2]*Department of Chemical Engineering and Biotechnology, University of Cambridge, Cambridge, UK*

[3]*Department of Chemistry, University of Cambridge, Cambridge, UK*

Misfolding and aggregation of proteins are characteristics of a range of increasingly prevalent neurodegenerative disorders including Alzheimer's and Parkinson's diseases. In Parkinson's disease and several closely related syndromes, the protein α-synuclein (AS) aggregates and forms amyloid-like deposits in specific regions of the brain. Fluorescence microscopy using fluorescent proteins, for instance the yellow fluorescent protein (YFP), is the method of choice to image molecular events such as protein aggregation in living organisms. The presence of a bulky fluorescent protein tag, however, may potentially affect significantly the properties of the protein of interest; for AS in particular, its relative small size and, as an intrinsically unfolded protein, its lack of defined secondary structure could challenge the usefulness of fluorescent-protein-based derivatives. Here, we subject a YFP fusion of AS to exhaustive studies *in vitro* designed to determine its potential as a means of probing amyloid formation *in vivo*. By employing a combination of biophysical and biochemical studies, we demonstrate that the conjugation of YFP does not significantly perturb the structure of AS in solution and find that the AS-YFP protein forms amyloid deposits *in vitro* that are essentially identical with those observed for wild-type AS, except that they are fluorescent. Of the several fluorescent properties of the YFP chimera that were assayed, we find that fluorescence anisotropy is a particularly useful parameter to follow the aggregation of AS-YFP, because of energy migration Förster resonance energy transfer (emFRET or homoFRET) between closely positioned YFP moieties occurring as a result of the high density of the fluorophore within the amyloid species. Fluorescence anisotropy imaging microscopy further demonstrates the ability of homoFRET to distinguish between soluble, pre-fibrillar aggregates and amyloid fibrils of AS-YFP. Our results validate the use of fluorescent protein chimeras of AS as representative models for

*Corresponding authors. C. W. Bertoncini is to be contacted at the Department of Chemistry, University of Cambridge, Lensfield Road, Cambridge CB2 1EW, UK. E. A. A. Nollen, Department of Genetics, University of Groningen, Oostersingel entrance 47, 9700 RB Groningen, The Netherlands. E-mail addresses: e.a.a.nollen@medgen.umcg.nl; cwb32@cam.ac.uk.

Present address: T. J. van Ham, Cardiovascular Research Center, Massachusetts General Hospital, Harvard Medical School, 149 13th Street, Charlestown, MA 02129, USA.

Abbreviations used: AS, α-synuclein; YFP, yellow fluorescent protein; FAIM, fluorescence anisotropy imaging microscopy; ThT, thioflavin T; TEM, transmission electron microscopy; CR, Congo red; HSQC, heteronuclear single quantum coherence; BS, β-synuclein; GFP, green fluorescent protein; emFRET or homoFRET, energy migration Förster resonance energy transfer.

studying protein aggregation and offer new opportunities for the investigation of amyloid aggregation *in vivo* using YFP-tagged proteins.

Edited by S. Radford

Introduction

Parkinson's disease and dementia with Lewy bodies are characterized by the deposition of cytoplasmic, protein-rich inclusions in certain regions of the brain, known as Lewy bodies.[1] The major constituent of such deposits is the 140-residue protein α-synuclein (AS), together with several minor components such as chaperones and ubiquitin.[2] Direct evidence for the involvement of AS in disease arises from the identification of point mutations and duplication of the AS locus linked with the early onset of neurodegeneration.[3–7] The biological function of AS appears to be related to synaptic plasticity by enhancing the priming step in the formation of synaptic vesicles, directly acting on the folding of SNARE proteins, possibly as a chaperone.[8] Gene knock-out studies have shown, however, that AS is not an essential protein, at least in rodents, which strongly suggest that the link to disease arises from a toxic gain of function.[9] AS is intrinsically unfolded in the cytoplasm but acquires substantial α-helical structure in its first 100 residues upon binding to lipid membranes.[10,11] Although it lacks defined secondary structure, long-range tertiary interactions exist and may help to prevent it from misfolding and aggregation to form amyloid deposits.[12–15] Interestingly, however, amyloid fibrils may not represent the species most toxic to neurons; instead, soluble oligomeric species and insoluble pre-fibrillar precursors to such fibrils appear to generate toxicity in cells.[16–20]

The vast majority of studies on amyloidogenic proteins have been carried out *in vitro* or *ex vivo* with material extracted from living organisms, as a consequence of the lack of suitable means of addressing the process of protein oligomerization and conformational changes in intact living cells. Recent technical advances in fluorescence microscopy, however, provide a wealth of tools that are uniquely suited for probing heterogeneous and transient species in the complex environment of a cell.[21] Fluorescence imaging offers many advantages for the study of misfolding and amyloid formation, in particular as observations can be made both *in vitro* and *in vivo*, facilitating direct comparison between both environments. Indeed, several approaches, such as tetracysteine FlaSH-ReaSH tagging, fluorescent protein tagging, split-fluorescent protein reconstitution (BiFC), and PDZ conjugation, have been used successfully to image AS misfolding and fibrillization.[18,22–25] Of these techniques, fluorescent protein tagging is of special interest as fluorescent protein derivatives come in a variety

of spectral and photoswitchable variants that allow multicolor and high-resolution imaging.[21,26] Furthermore, fluorescent proteins are a very valuable tool for live imaging in whole organisms such as the nematode worm *Caenorhabditis elegans*, the fruit fly *Drosophila melanogaster*, and even mice. Indeed, many animal models of disease have been established, employing fluorescent protein tagging to study misfolding and accumulation of AS,[27–31] along with other misfolding disease-related proteins.[32–35]

Conjugation of proteins by fluorescent proteins may, however, perturb the native structure and function of the tagged protein given the bulkiness of the fluorescent moiety (∼28 kDa). In the case of AS, this may be of particular concern, not only because of its relatively small size (∼14 kDa) but also because of its lack of persistent structure in solution. It is possible, therefore, that fluorescent protein tagging may affect the intrinsic propensity of AS to form fibrils and thus render the conjugate less valuable than one might hope for studying the behavior of native AS. Not surprisingly, some controversy has been raised from studies of AS misfolding and aggregation using fluorescent proteins *in vivo*, and the validation of this system by biophysical techniques is essential. Here, we conduct a detailed biophysical characterization of AS tagged C-terminally with the yellow fluorescent protein variant Venus [36] (termed here AS-YFP) and investigate its use as a reporter of AS misfolding and aggregation. We further examine the fluorescence properties of aggregated AS-YFP and demonstrate the applicability of fluorescence anisotropy imaging microscopy (FAIM) in the characterization of amyloid aggregation of proteins.

Results

AS-YFP forms amyloid fibrils *in vitro* in a similar manner to wild-type AS

A fluorescent protein chimera of AS was constructed by fusing the YFP gene (named Venus) to the C-terminus of AS, separated by a short linker peptide (AlaProValAlaThr), designed to minimize any effects of the fusion process on both proteins.[35] To investigate the amyloid aggregation behavior of AS-YFP, we performed protein aggregation assays on the purified chimeric protein; as a control, wild-type AS was assayed in parallel. Both proteins were subjected to standard *in vitro* aggregation procedures, incubating the purified proteins at 37 °C with constant agitation. Aliquots were taken from both
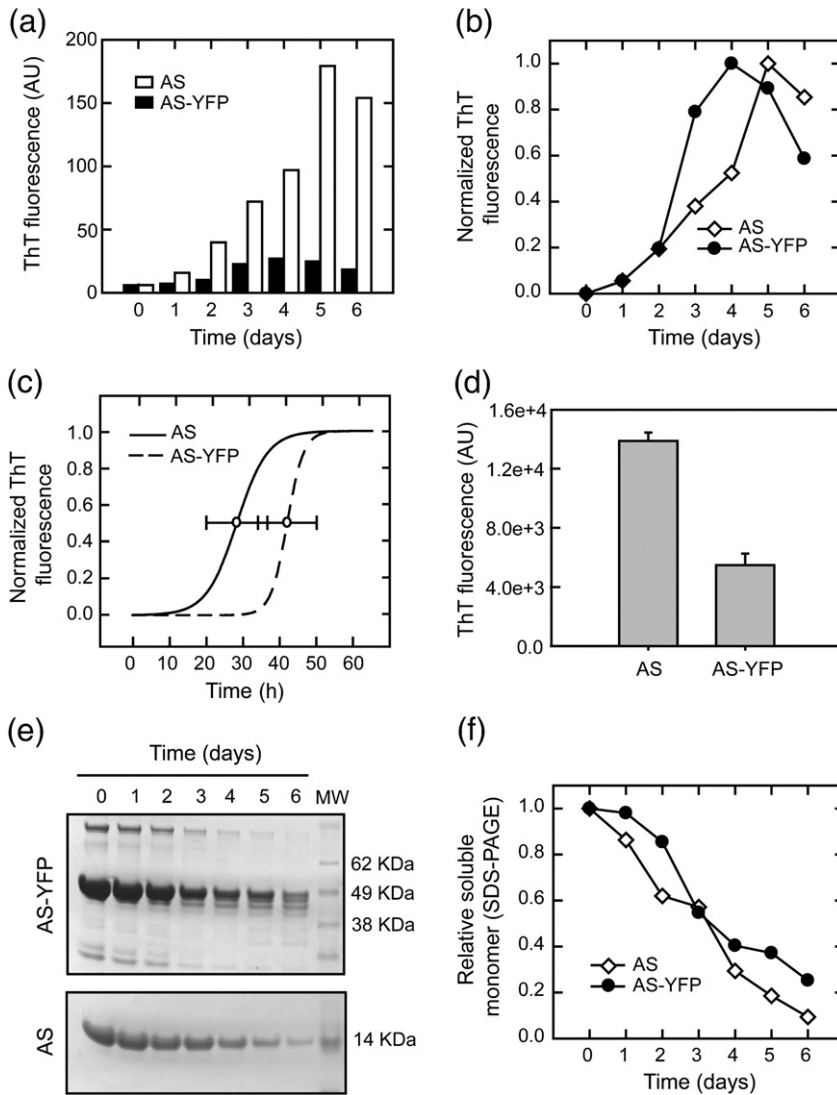
Fig. 1. AS-YFP and AS aggregate *in vitro* in a similar manner. Analysis of the aggregation kinetics of AS-YFP and AS. (a) ThT fluorescence for AS-YFP (filled bars) and AS (open bars). (b) Normalized ThT fluorescence for AS-YFP (filled circles) and AS (open diamonds). (c) Aggregation kinetics of AS-YFP (continuous line) and AS (broken line) in the presence of SDS. Plotted are time traces of fitted average ThT fluorescence traces. The standard deviation of the lag phase is indicated with errors bars. (d) Absolute ThT fluorescence intensity of AS-wt and AS-YFP at the endpoint of the SDS-containing aggregation assay. (e) SDS-PAGE of the soluble fraction obtained by high-speed centrifugation of the samples withdrawn at each time point of the assay shown in (b). (f) Densitometry analysis of the amount of soluble protein remaining as resolved by SDS-PAGE in (d), for AS-YFP (filled circles) and AS (open diamonds).

samples every 24 h during the aggregation time course to measure binding of thioflavin T (ThT) and to examine the aggregate morphology by transmission electron microscopy (TEM). ThT is an amyloid-sensitive dye, which develops fluorescence at 480 nm upon binding to the β-sheet-rich amyloid fibrils.[37] Moreover, the analysis of the normalized time dependence of the ThT fluorescence intensity allows the kinetics of amyloid formation to be defined for the proteins under investigation. Upon aggregation, both AS-YFP and AS samples show increasing ThT fluorescence, indicative of amyloid formation (Fig. 1a).

The kinetics of the fluorescence rise were found to be similar for the two proteins (Fig. 1b), although at the end of the assay, the ThT signal of AS-YFP was considerably lower in intensity than that of AS (by 85%). This latter effect can be attributed either to hampered binding of the dye in the presence of YFP or to the transfer of energy between the two fluorophores. Indeed, significant energy transfer between ThT and YFP was observed in the aggregates (data not shown), arguing against

utilization of ThT binding as the sole indicator of protein aggregation in this case. Still, both proteins display similar aggregation kinetics, with the AS-YFP protein aggregating slightly faster than the wild-type protein. We also probed the aggregation of AS-YFP in the presence of SDS, a membrane-mimetic environment, since lipids have been proposed to mediate AS inclusion formation *in vivo*.[38] In the presence of SDS, AS-YFP amyloid formation was slightly retarded in comparison to AS (halftime for aggregation was 42 ± 8 h for AS-YFP *versus* 29 ± 8 h for AS). Again, the final ThT intensity in AS-YFP aggregates was reduced, reaching only 35% of that in the wild-type protein (Fig. 1c and d). To estimate the amount of protein aggregated in a ThT-independent manner, we determined the relative amount of soluble protein at each time point of the assay; the supernatants of each sample were analyzed by SDS-PAGE after centrifugation at 13,000 rpm to remove aggregated species. Both AS and AS-YFP showed a time-dependent decrease in the quantity of protein remaining in solution by SDS-PAGE (Fig. 1e), and densitometric analysis of
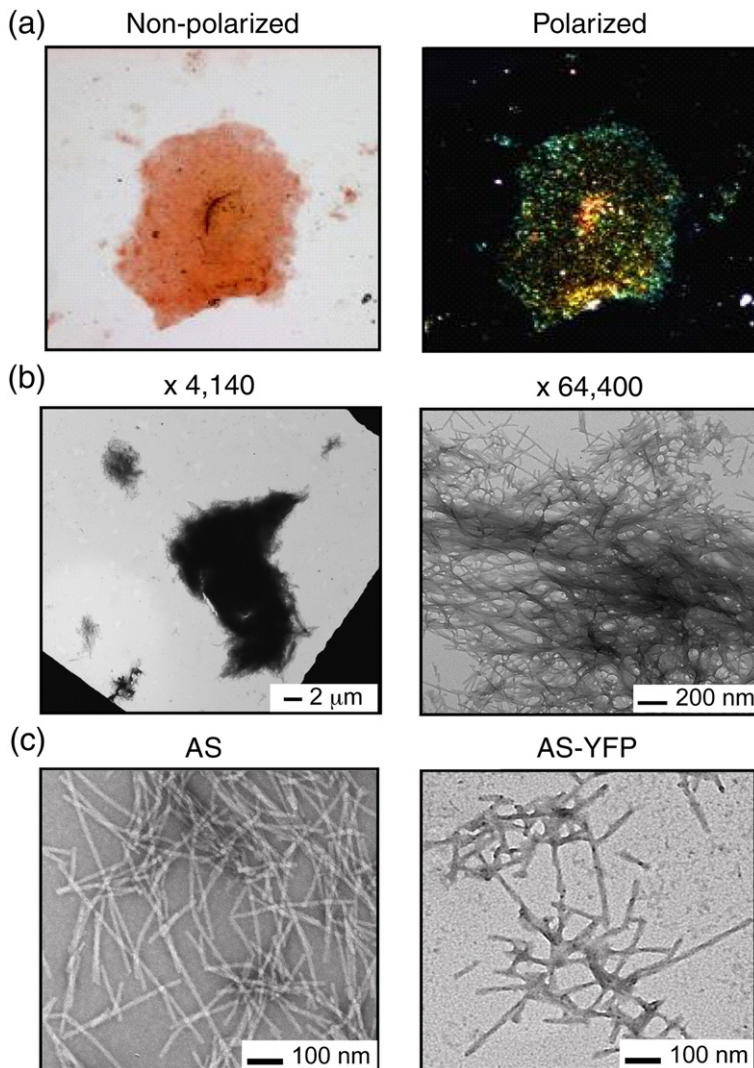
Fig. 2. AS-YFP and AS form amyloid-like deposits *in vitro*. (a) Aggregated AS-YFP at day 5 showing apple-green birefringence when visualized by polarized light upon CR binding. (b) TEM images of AS-YFP. Note the very densely packed aggregated material, with fibrils stemming out. (c) High-magnification TEM images showing the detailed fibrillar morphologies for AS and AS-YFP.

the gel bands shows that the rate of aggregation was comparable for both proteins, indicative of similar aggregation kinetics (Fig. 1f).

Next, we assayed the AS-YFP aggregates for binding of Congo red (CR), an amyloid-specific dye that binds to the β-sheet-rich structure of the fibrils and displays apple-green birefringence upon exposure to polarized light.[37] Aggregated AS-YFP shows, like AS itself, this characteristic birefringence when stained by CR, further indicating the amyloid-like character of these deposits (Fig. 2a). To assess the structure of the amyloid deposits of AS-YFP, we analyzed the samples by TEM. Amyloid-like fibrils were observed in the AS-YFP sample, which are comparable in width and length to AS fibrils (Fig. 2b). Very densely packed aggregates were also observed in the AS-YFP sample, however, with fibrils stemming out from them, which suggests an enhanced cluster of the fibrils with YFP attached. The AS-YFP filaments obtained were straighter than those of AS, and the characteristic twist was not readily observed in these fibrils, due to insufficient contrast enhancement after negative staining (Fig. 2c). This effect could be a consequence of the

conjugated YFP molecule; indeed, detailed analysis of the morphology of AS-YFP deposits shows that the fibrils have irregular edges, probably reflecting the attachment of the flexibly linked YFP moiety. Analysis of the width of individual fibrils shows no differences between wild-type AS and AS-YFP (17 ± 3 nm *versus* 16 ± 2 nm, respectively). Moreover, in both cases, fibrils typically reached between 500 nm and 1 μm in length. Taken together, these results provide strong evidence that AS-YFP forms amyloid-like fibrils with similar properties to AS.

NMR spectroscopy demonstrates that YFP fusion does not perturb the structural properties of AS

We next investigated whether the conjugation of YFP alters the structural properties of AS in solution. To probe the conformation of AS-YFP with residue-specific resolution, we employed heteronuclear NMR spectroscopy with isotopically labeled (^{15}N) AS and AS-YFP. The ^{1}H–^{15}N heteronuclear single quantum coherence (HSQC) spectrum of AS-YFP is essentially identical with that of AS, with only minor
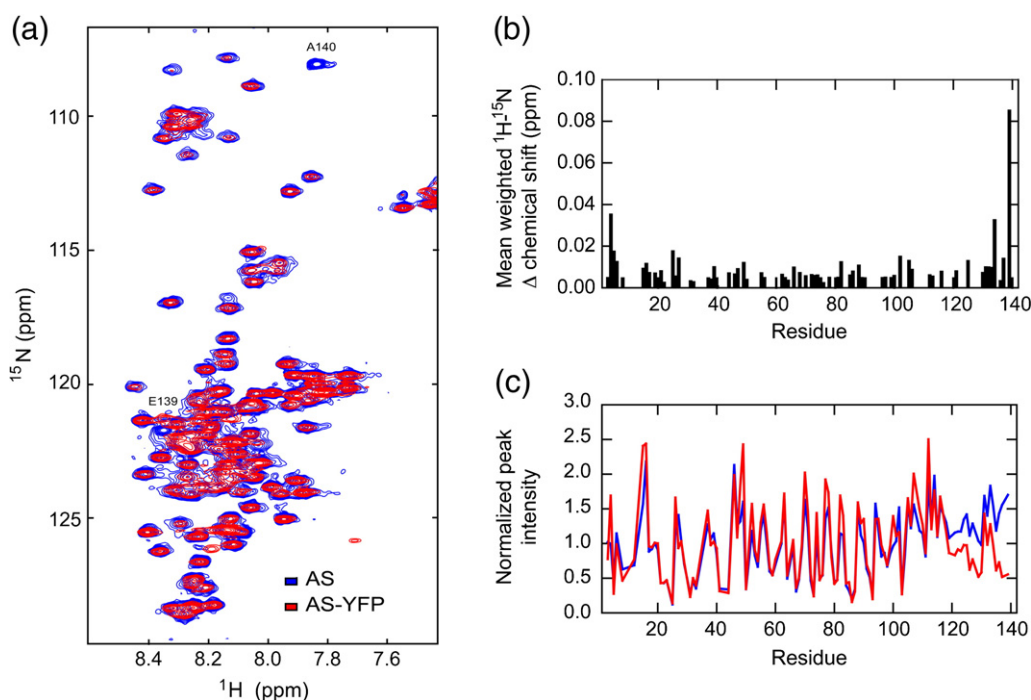
Fig. 3. NMR demonstrates that the YFP fusion does not significantly perturb the backbone structure of AS. (a) Overlaid ^{1}H–^{15}N HSQC spectra of AS (blue) and AS-YFP. (b) Mean weighted chemical shift differences for backbone ^{1}H–^{15}N resonances between AS and AS-YFP. (c) Normalized ^{1}H–^{15}N HSQC peak intensities for AS (blue) and AS-YFP (red).

(<0.1 ppm) chemical shift differences located at the very end of the C-terminus, where the YFP moiety is attached (Fig. 3a and b). A few small (<0.04 ppm) chemical shifts are also observed for N-terminal residues but can be attributed to a slight variation in the pH of the samples. A comparison of the normalized intensities of ^{1}H–^{15}N cross peaks, a parameter highly sensitive to changes in the dynamics of the conformation of AS and its interaction with the solvent,[39–41] revealed more subtle YFP-mediated perturbations to the C-terminal region of the protein comprising residues 120 to 140 (Fig. 3c). Overall, therefore, the observed structural and dynamical perturbations are minor and restricted to the local region in which the YFP has been attached.

Only a very few YFP peaks, all with low intensity, are observed in the HSQC spectra of AS-YFP, an effect attributable to the large line widths of these resonances due to the size and, hence, slow tumbling rate ($\tau_C \sim 20$ ns) and relaxation properties of this folded region of the construct. These effects are particularly significant for experiments conducted at such low temperature (10 °C), chosen to enable clear detection of resonances of the monomeric AS. A recent NMR study of isolated YFP was successfully conducted using a sample that was 10 times more concentrated than that used here, and at 37 °C, thereby increasing the tumbling rate of the YFP and reducing the peak line widths.[42] Indeed, when the temperature of the AS-YFP sample was increased to 37 °C, YFP peaks were detectable in the HSQC spectrum (Supplementary Fig. 1); the AS resonances

were, however, severely diminished relative to those at 10 °C due to solvent exchange properties.[40,41]

AS-YFP but not BS-YFP forms fluorescent amyloid-like aggregates

We next set out to address the possibility of fluorescent-protein-mediated interactions in the aggregation of AS-YFP and therefore studied a YFP chimera of β-synuclein (BS-YFP), the somewhat less amyloidogenic homologue of AS. BS lacks a stretch of hydrophobic residues within the central region of the protein, a property that is believed to contribute, along with some more specific residue-specific factors, to its very low aggregation propensity.[43,44] Indeed, BS does not detectably aggregate at physiological conditions in aqueous solution, even after long periods of time, and has in addition been shown to inhibit amyloid formation by AS.[45,46] Based on these studies, BS-YFP is not expected to form fibrils under conditions relevant to studies of AS aggregation and constitutes an effective negative control for our *in vitro* studies.

When subjected to our standard *in vitro* fibrillization assay (37 °C and shaking), AS-YFP, but not BS-YFP, formed insoluble fluorescent aggregates (Fig. 4a). Quantitative determination of the YFP fluorescence in the samples showed that, simultaneously with the appearance of aggregates in the AS-YFP sample, YFP fluorescence was depleted from the soluble fraction, falling to less than 20% by the end of the assay (Fig. 4b). Experiments with BS-YFP, by contrast, showed that 90% of its YFP
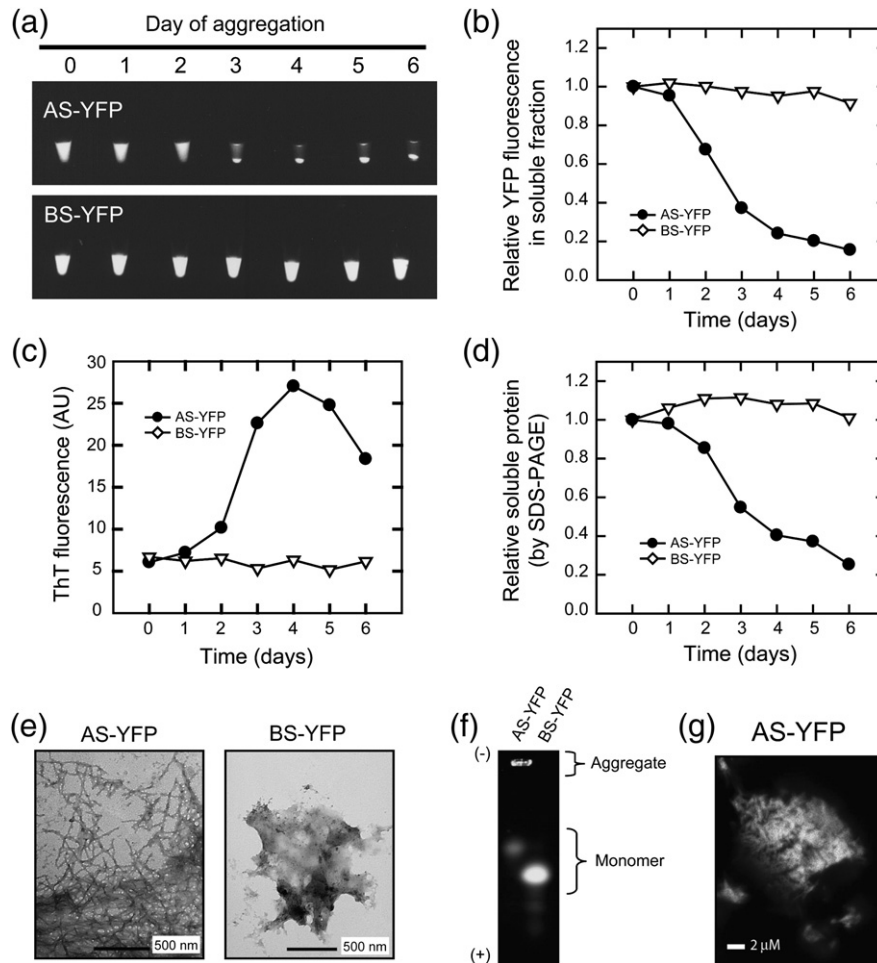
Fig. 4. AS-YFP but not BS-YFP forms fluorescent amyloid-like aggregates. Analysis of the aggregation kinetics of AS-YFP and BS-YFP. (a) UV excitation of aliquots withdrawn from the aggregation assays on a daily basis. (b) Relative fluorescence intensity of the soluble fraction obtained by high-speed centrifugation of samples shown in (a). (c) ThT fluorescence of the samples shown in (a). (d) Densitometry analysis of the amount of soluble protein detected by SDS-PAGE. (e) TEM image of aggregated protein present at the endpoint of the aggregation assay. (f) In-gel visualization of YFP fluorescence of aggregated AS-YFP and BS-YFP (day 6) separated on a native agarose gel (1%). (g) Confocal fluorescence image of an AS-YFP deposit (60× oil objective, 10× digital zoom). In all the plots, AS-YFP is represented as filled circles and BS-YFP is represented as open triangles.

fluorescence is retained in the soluble fractions at the endpoint of the assay. In line with the absence of aggregated material, no ThT binding was detected in the BS-YFP sample (Fig. 4c). Furthermore, SDS-PAGE analysis of the soluble fraction demonstrated that the concentration of BS-YFP protein remained essentially constant during the assay, in contrast to experiments with AS-YFP in which soluble protein concentration decreased by some 75% at the end of the assay (Fig. 4d).

Consistent with these findings, no fibrils could be found by TEM in solutions in which a BS-YFP sample was incubated for 6 days, whereas fibrils were the predominant species observable in the AS-YFP sample (Fig. 4e). Native gel electrophoresis showed that AS-YFP samples remained in the loading well of the gel whereas BS-YFP migrated through the gel and could be resolved, indicating the presence of aggregated fluorescent material solely in the AS-YFP sample (Fig. 4f). Finally, we

explored the feasibility of imaging AS-YFP aggregates in a confocal fluorescence microscope. Deposits of AS-YFP were easily identified on a microscope slide given their brightness, and it was even possible to observe some structural features of the aggregates, despite the low resolution of the confocal microscope when compared with TEM (Fig. 4g). Taken together, these data indicate that amyloid deposits of AS-YFP remain fluorescent and can be imaged and that fibril formation results from the amyloidogenic character of the AS protein rather than from interactions mediated by YFP.

Characterization of the fluorescent properties of fibrillar deposits of AS-YFP

We next focused our studies of AS-YFP by assessing its spectral properties during amyloid formation. Both AS-YFP and BS-YFP exhibit fluorescence excitation and emission spectra that are

indistinguishable from those of the isolated YFP (Supplementary Fig. 2a). In general, fluorescence of this particular YFP variant (Venus) is less sensitive to the environment than is the fluorescence of the rest of the fluorescent proteins, but it is still possible that properties such as the spectrum and the fluorescence intensity could be altered upon protein aggregation.[36] Indeed, some variations in the fluorescence properties of AS-YFP were observed during the aggregation time course, in a manner that was dependent on the fraction of protein aggregated (Fig. 5). Analysis of the fluorescence emission

spectra of the samples during different time points of the aggregation assay shows that approximately 50% of the AS-YFP fluorescence is quenched upon amyloid formation (Fig. 5a). As expected, the fluorescence of the soluble fraction was also reduced, consistent with the decrease of monomeric AS-YFP protein in the supernatant (Fig. 5b and c).

Comparison of the spectra of the soluble and aggregated forms of the protein revealed a spectral red shift of 2 nm upon AS-YFP aggregation (Fig. 5c and d). This small shift is indicative of the occurrence of inner filter effects (i.e., reabsorption of emitted
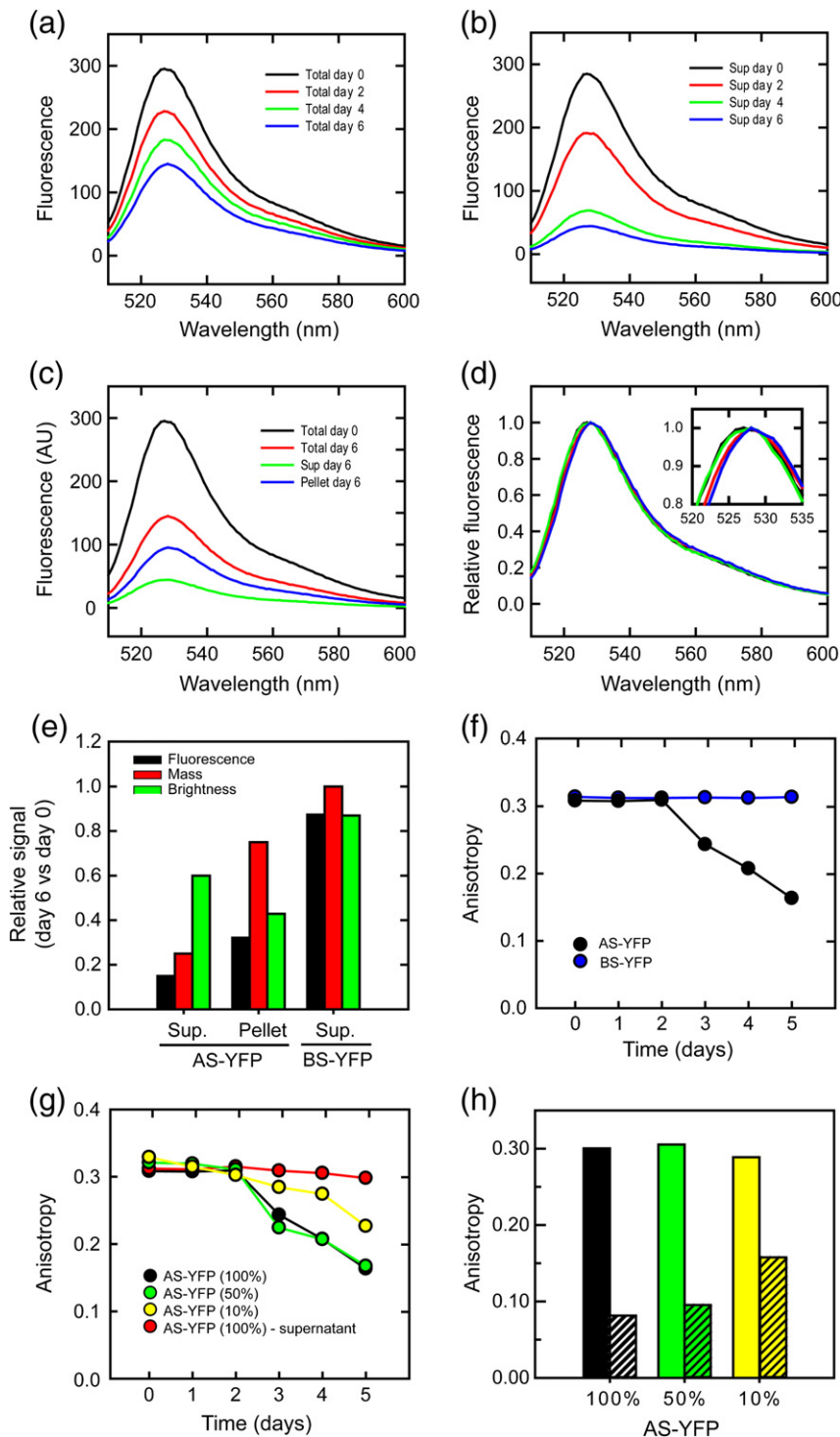

Fig. 5. Characterization of the spectral properties of fibrillar deposits of AS-YFP. AS-YFP was allowed to aggregate and the fluorescence properties of the YFP molecule were measured. (a and b) Fluorescence spectra of total fraction (a, total) or soluble fraction (b, supernatant) of AS-YFP at different time points during aggregation: day 0 (black), day 2 (red), day 4 (green), and day 6 (blue). (c) Fluorescence spectra of soluble *versus* aggregated AS-YFP: total sample day 0 (black), total sample day 6 (red), soluble fraction day 6 (green), aggregated fraction day 6 (blue). (d) Normalized data shown in (c), highlighting a 2-nm spectral shift between the soluble and aggregated AS-YFP (inset). (e) Relative fluorescence intensity per unit of mass (brightness) of soluble and aggregated AS-YFP at the endpoint of the time course (day 6) with respect to the initial sample (day 0): the relative brightness is calculated as the ratio of fluorescence intensity (red) over the mass of protein aggregated (black). The data for BS-YFP spectral characteristics at the endpoint of the assay are shown for comparison. (f) Time-dependent determination of fluorescence anisotropy in the aggregated samples of AS-YFP (black) and BS-YFP (blue). (g) HomoFRET is the cause for loss of anisotropy upon aggregation in AS-YFP. Time dependence of the fluorescence anisotropy corresponding to aggregating pure AS-YFP (100%, black) and samples containing a fraction of AS (50%, green, and 90%, yellow). In red, change in fluorescence anisotropy for the soluble fraction of AS-YFP (100%) at each time point of the assay. (h) Comparison of the fluorescence anisotropy of the soluble (plain bar) and aggregated (hatched bar) fractions corresponding to samples in (g) at the end of the aggregation assay.

light) due to the high local concentration of fluorophores in the aggregate.[47,48] A time-dependent reduction in brightness, that is, the relative change in fluorescence intensity per unit mass, of AS-YFP also accompanied amyloid formation, resulting in a decrease of ~60% relative to that of monomeric AS-YFP at the end of the assay (Fig. 5e and Supplementary Fig. 2b). In addition to the above-mentioned inner filter effect, we note that absorption flattening (i.e., reduced absorption of photons by the chromophores due to shielding effects at high concentrations) is likely to be another major optical effect limiting the excitation of the YFP fluorophore in the aggregated sample.[49] Reduced fluorescence intensity could also result from the misfolding of a partial population of YFP molecules in the fibril state, as reported for some green fluorescent protein (GFP) chimeras of amyloidogenic peptides,[35] giving rise to a decrease in the extinction coefficient and quantum yield of the fluorophore. Absorption spectroscopy showed, however, that aggregated AS-YFP maintains the ratio of both chromophore/aromatics absorbance and YFP fluorescence/absorbance compared to monomeric AS-YFP, suggesting that misfolding of YFP is not a major cause for the decrease in brightness in this case (Supplementary Fig. 2c–f). As a control, we followed the variation in fluorescence intensity for BS-YFP during the aggregation assay and found that 90% of the brightness was retained and no spectral shift was evident (Supplementary Fig. 2c–f). This result is in line with BS-YFP remaining essentially soluble and monomeric throughout the time course of aggregation.

Another fluorescence-based phenomenon that could occur upon self-association of AS-YFP is energy transfer between the identical YFP molecules, termed energy migration Förster resonance energy transfer (emFRET) or homoFRET. Energy migration between the same type of molecule typically occurs for fluorophores that display small Stokes shift (i.e., which have a high overlap between their excitation and emission spectra) and is readily observed as a decrease in steady-state anisotropy of the fluorophore.[48,50] Indeed, homoFRET between fluorescent proteins has been used previously to study protein oligomerization *in vitro* and in the cellular environment.[51] When we measured the steady-state fluorescence anisotropy of AS-YFP and BS-YFP along the aggregation time course, we observed a strong decrease in anisotropy for the AS-YFP sample concomitant with the formation of amyloid fibrils, a result indicative of the occurrence of energy migration between identical molecules (Fig. 5f). Anisotropy in a solution containing only monomeric AS-YFP (day 0) was ~0.31, similar to the value of untagged YFP (0.30) and BS-YFP (0.32). This parameter then decreased to 0.16 at the endpoint of the assay for the AS-YFP sample, while it remained constant for BS-YFP.

If the observed loss of anisotropy is a consequence of homoFRET, it should be sensitive to the extent of labeling with the fluorophore, as energy migration depends on the distance between the acceptor and

donor fluorophores.[50] In order to demonstrate that homoFRET is the dominant phenomenon causing depolarization, we performed aggregation experiments in samples containing different ratios of AS-YFP and AS. At the endpoint of the aggregation assay in a sample containing 10% AS-YFP and 90% AS, the loss of anisotropy was reduced to an endpoint value of 0.22, indicating that homoFRET is indeed the prevalent mechanism for depolarization (Fig. 5g). Interestingly, a 50% AS-YFP sample showed a similar time-dependent decrease in anisotropy as the 100% AS-YFP sample, revealing an extremely high efficiency of energy migration that must arise from the close proximity of the YFP molecules in the aggregates (Fig. 5g). The conclusion that the insoluble amyloid fraction is responsible for the lower anisotropy registered in the sample is further verified by measuring the anisotropy of the isolated soluble and insoluble fractions at the endpoint of the aggregation time course (Fig. 5f–h). The anisotropy of the insoluble fraction (in buffer suspension) for a 100% AS-YFP sample reached 0.08, while it increased slightly for the samples containing AS, as a function of the decrease in fluorophore concentration (0.09 for 50% AS-YFP and 0.16 for 10% AS-YFP). Taken together, these fluorescence anisotropy studies strongly indicate the occurrence of homoFRET between neighboring YFP molecules in the aggregated state of AS-YFP.

FAIM of AS-YFP probes amyloid formation

The final step in our studies was aimed to explore the feasibility of anisotropy-based identification of amyloid deposits in a microscope, exploiting the phenomena of homoFRET. FAIM of soluble monomeric AS-YFP showed the expected value of 0.31, while aggregated AS-YFP evidenced a significant decrease in anisotropy, down to 0.10, due to the strong occurrence of homoFRET in the amyloid state (Fig. 6a–c). Pixel-based analysis of the images allowed us to investigate the anisotropy of the aggregates with high spatial resolution, a parameter that turned out to be very homogeneous throughout all the deposits examined (Fig. 6b). Notably, we found a very close correlation between the value of the anisotropy obtained by using a spectrofluorometer (Fig. 5h) and that determined in the studies using FAIM, strongly supporting the validity of the observations.

The usefulness of the fluorescent protein derivative of AS in FAIM is revealed by comparison to a derivative tagged with the small organic fluorophore Alexa-488 (AS-A488). Because of its short rotational correlation time, this fluorophore has a very low anisotropy in solution ($r < 0.02$) (Fig. 6d). Upon aggregation, the anisotropy of AS-A488 increased to 0.09. Although significant, the contrast between the soluble and aggregated form of AS-A488 is limited in comparison to that observed for AS-YFP. Indeed, the increase in anisotropy resulting from the increase in rotational correlation time associated with aggregation is counteracted by the efficient homoFRET between closely spaced Alexa-488
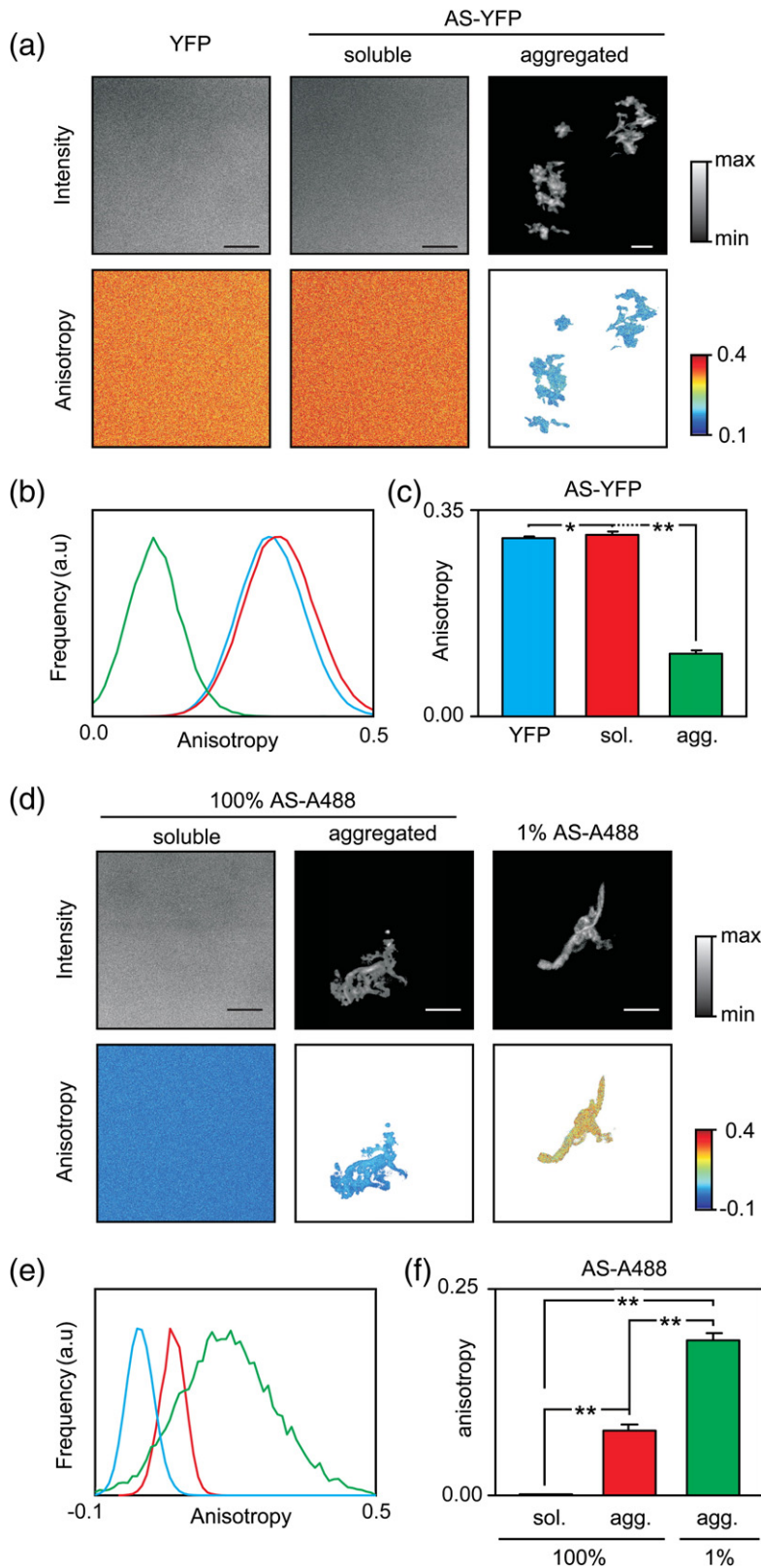
Fig. 6. Fluorescence anisotropy imaging detects amyloid formation by AS-YFP. (a) Intensity (top) and anisotropy images (bottom) of soluble YFP (left), soluble AS-YFP (middle), and aggregated AS-YFP (right). A reduction of anisotropy is evident following aggregation as shown also by the anisotropy histograms (b) and statistical analysis (c). (d)–(f) show the same measurements, but with AS-Alexa 488. Note that the broad distribution of anisotropy (e) for the 1% AS-488 sample is caused by the lower concentration of fluorophores, which result in lower signal-to-noise ratios, rather than representing an effect of biological significance. The scale bar represents 5 μm.

molecules. Utilization of a sample containing only 1% of labeled protein impaired energy transfer and did allow a much better assessment of differences between soluble and aggregated AS-A488 (anisotropy ~0.19) employing fluorescence anisotropy imaging (Fig. 6e and f). This approach, however, requires a much higher laser power, increases the noise in the images, and is not readily applicable *in vivo*, highlighting the usefulness of the AS-YFP chimera.

FAIM was also employed to assess pre-fibrillar aggregates occurring during the process of AS-YFP amyloid formation, suggested to contain aggregation

species toxic to neurons.[17,52] AS-YFP aggregated *in vitro*, at a relatively low protein concentration (50 μM), showed an extended lag phase (6 days) allowing for visualization of aggregation intermediates by FAIM and TEM on a daily basis (Fig. 7). As observed by TEM, almost no aggregated material was found at day 2 of the assay, whereas pre-fibrillar aggregates were

observed from day 4. The highest amount of pre-fibrillar aggregates was observed at day 6, after which predominantly amyloid fibrils were observed (day 8) (Fig. 7a). Pre-fibrillar aggregation intermediates of AS-YFP (days 4–6) displayed much lower fluorescence than mature amyloid deposits (day 8) but higher than the monomeric protein in solution, a sign of the
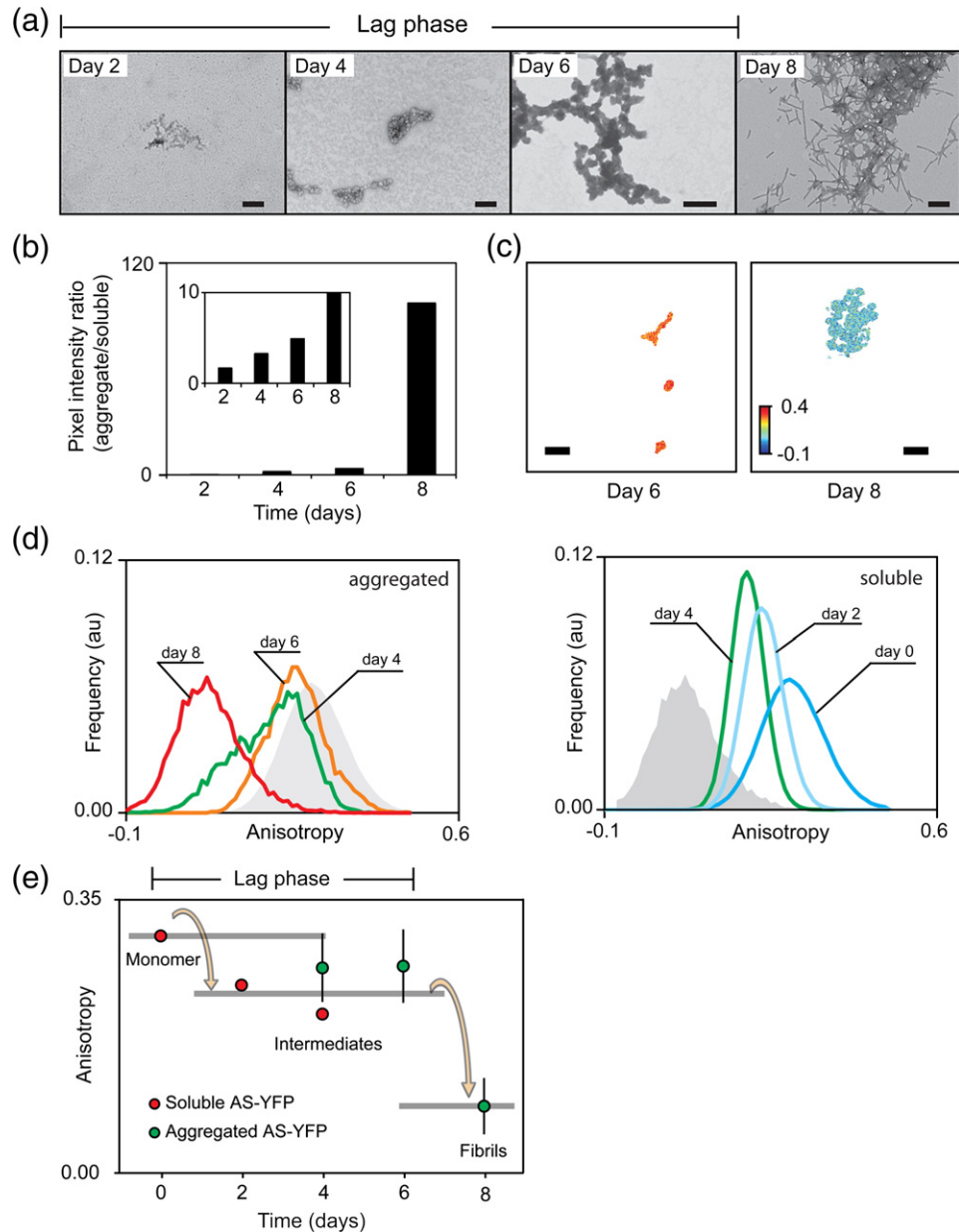

Fig. 7. The aggregation pathway of AS-YFP as visualized by fluorescence anisotropy microscopy. (a) Representative TEM images corresponding to the aggregation intermediates populated during AS-YFP amyloid fibril formation. Scale bars represent 200 nm. (b) Pixel intensity ratio for aggregated/soluble species along the aggregation pathway determined from the confocal fluorescence anisotropy images. Note how the pixel intensity ratio in amyloid deposits (day 8) is particularly high as a consequence of both fluorophore density and reduced soluble protein remaining. (c) Confocal fluorescence anisotropy image corresponding to AS-YFP pre-fibrillar aggregates (day 6) and deposits of amyloid fibrils (day 8). The scale bar represents 5 μm. (d) Anisotropy histograms of soluble (left) and aggregated (right) fractions at various time points during the fibrillation of AS-YFP. Anisotropy for soluble and aggregated fractions was determined from the analysis of different regions of interest in the same image. In gray, anisotropy histograms corresponding to amyloid (right) and the initial soluble species (left) are shown as references. (e) Plot of average anisotropy for soluble and aggregated AS-YFP determined from the global analysis of the images. Circles represent average of averages for individual images. Error bars correspond to the standard deviation of the average.

high density of fluorophores present in the aggregated state (Fig. 7b). Notably, FAIM showed that fluorescence anisotropy of such pre-fibrillar aggregates remained considerably high (~0.27) in contrast to amyloid deposits of AS-YFP, which displayed strongly decreased anisotropies of about 0.10 (Fig. 7c).

Therefore, because soluble and aggregated protein can be distinguished based on fluorescence intensity, the anisotropy for different species could be measured within the same FAIM image (Fig. 7d and e). A decrease in anisotropy for soluble AS-YFP species compared to the monomeric protein was observed, particularly at day 4, indicative of efficient transfer of energy between AS-YFP molecules, probably due to the presence of fast exchanging diffusive small oligomeric species.[53] Pre-fibrillar insoluble species (days 4 to 6) showed, surprisingly, higher anisotropy than soluble oligomeric AS-YFP, indicative of a less efficient transfer of energy. The apparent reduced occurrence of homoFRET within pre-fibrillar aggregates compared to soluble oligomers is not related to a low degree of compactness in the former but likely reflects the YFP adopting certain preferential orientations in the aggregates that precludes efficient transfer of energy (see Discussion). In amyloid fibrils, conversely, the efficiency of energy transfer is maximal, suggestive of a very densely packed and ordered state. These data demonstrate the applicability of FAIM to distinguish between aggregation intermediates and mature amyloid fibrils *in vitro* and the remarkable potential of the technique to investigate amyloid formation *in vivo*.

Discussion

During the past decade, a large number of studies have addressed the amyloid-forming capabilities of AS and the toxicity of intermediates in the aggregation pathway.[17,54] The mechanisms by which AS aggregation, in a cellular context, causes degeneration of dopaminergic neurons are, however, not well understood. One of the reasons that studies of AS aggregation *in vivo* are very challenging is that it is difficult to characterize the heterogeneous aggregated AS species in tissue, a task for which multiparametric fluorescent imaging is ideally suited.[55,56]

Several studies have already employed fluorescent protein fusions to probe AS misfolding, aggregation, and toxicity in a wide range of model organisms and cells in culture. In yeast cells, AS-GFP localizes first in the plasma membrane, after which it accumulates into small fluorescent cytoplasmic inclusions that consist of vesicular clusters.[18,38] The expression of AS-GFP causes a defect in membrane trafficking as a first sign of toxicity in yeast cells,[31] and non-fibrillar lipid-rich AS-GFP deposits are observed in such models. In another study, AS-GFP was expressed in a neuronal cell line and in mouse brains, and in this case, discrete granular fluorescent aggregates were found both in cells and in tissue.[29] Indeed, in the brain, electron-dense bodies and vacuolar structures indicative of neurodegeneration were also observed. In *C. elegans*,

we and others recently reported that AS-YFP inclusions accumulate during aging;[27,28] in old age animals, the deposition of AS-YFP into immobile aggregates was revealed by a lack of recovery of YFP fluorescence following laser-induced photobleaching.[27] In such studies of AS amyloid formation, however, the relative small size and unfolded nature of AS could question the reliability of fluorescent protein tagging. For this reason, we considered that a detailed biophysical characterization of the fused protein was required for the validation of the findings drawn from these models of disease and for the development of fluorescence microscopy-based assays employing fluorescent-protein-tagged AS.

Our detailed biophysical study of the AS-YFP fusion protein demonstrates that this protein is a very robust model of AS amyloid formation for the following reasons: (1) AS-YFP forms amyloid-like fibrils comparable to those formed by the native AS protein; (2) AS-YFP deposits show ThT and CR binding characteristic of amyloid formation; (3) the kinetics of amyloid formation are similar for AS and AS-YFP in the presence and absence of lipid mimetics; (4) the YFP moiety attached to the C-terminus of AS does not perturb significantly the structure of the protein; and (5) the aggregation of AS-YFP is solely triggered by the amyloidogenicity of AS. The similarity in the behavior of the C-terminally tagged YFP fusion can be explained, at least in part, by the fact that the C-terminus of AS, rich in proline residues, is not incorporated into the amyloid structure and remains disordered and in solution.[57–59] Our studies establish in addition that the BS-YFP chimera should constitute a valuable negative control for amyloid-related *in vivo* studies, since it does not form fibrillar aggregates *in vitro* under the conditions assayed.

From a methodological point of view, the results of this study highlight the fact that the fluorescence properties of the YFP moiety can be exploited as a valuable probe through which to assess the aggregation state of AS, not only in isolation but also in imaging studies using multiparametric fluorescence microscopy. Upon amyloid formation, the fluorescence emission maximum of AS-YFP displays a slight red shift, probably reflecting the occurrence of inner filter effects as the protein coalesces into aggregates and increases its local concentration.[47,48] This conversion is also accompanied by a strong reduction in the brightness of the YFP moiety, causing a reduction in the apparent fluorescence intensity per YFP molecule in the aggregates of about 60%. Such spectral changes have been shown not to be indicative of a fraction of YFP in a misfolded non-fluorescent state, as has been suggested for amyloid deposits of the Alzheimer's Aβ peptide–GFP fusion[60] and other amyloidogenic peptides.[35] We cannot completely rule out, however, the presence of a small fraction of YFP in a dark state with similar absorption characteristics as soluble AS-YFP, but not fluorescent. Instead, the loss of fluorescence intensity in amyloid deposits of AS-YFP reports on the phenomena of absorption flattening and inner filter effects due to the high local density of fluorophores,

by which YFP molecules could "shadow" or reabsorb photons from neighboring molecules rendering the aggregate less fluorescent.[49]

The most sensitive YFP fluorescence parameter that reports on AS-YFP aggregation, however, appears to be fluorescence polarization anisotropy that results from homoFRET, a phenomenon of energy migration between fluorophores of the same chemical nature. Upon amyloid formation, AS-YFP shows strong homoFRET, measured as a decrease in steady-state fluorescence anisotropy, indicative of a very close proximity of the YFP molecules in the aggregated state. Such perturbations of the fluorescent properties of the YFP moiety are not observed for BS-YFP, indicating that these parameters are valuable probes of amyloid formation. We observed that ThT fluorescence is detected prior to changes in fluorescence anisotropy, probably because in the latter, the relative weight of the signal arising from the fibrils ($r<0.1$) is masked by the signal from the monomeric fraction ($r>0.3$). Anisotropy is very sensitive to the size and hydrodynamic properties of the fluorophore, in such a way that a rise in anisotropy occurs with an increase in size. In the system under study, two opposing effects contribute to the measured anisotropy: homoFRET, which reduces the anisotropy, and an increase in size due to oligomerization, which increases it. Time-resolved anisotropy measurements, in which rotational correlation times of individual species can be determined, would therefore allow the tracking of the oligomerization state of AS-YFP at early stages of aggregation, as previously shown for other amyloid species, including pyrene-labeled AS.[61,62] The short fluorescent lifetime of the YFP fluorescence ($\tau \sim 3$ ns) is, however, not likely to provide a window of time resolution long enough to probe large oligomeric species, due to the fact that their rotational correlation times would be much larger than the lifetime of the fluorophore.

Interestingly, a property such as homoFRET can be easily exploited in FAIM, providing extra resolution for the investigation of molecular interactions by means of microscope-based anisotropy measurements.[63] In fact, the occurrence of homoFRET has been used previously to assess the oligomerization state of several proteins in living cells, indicating that such fluorescence anisotropy measurements should enable amyloid formation to be probed *in vivo*.[64,65] Indeed, simply using a polarization beam splitter cube at the output port of a standard confocal microscope permits the simultaneous resolution of the parallel and perpendicular components of the fluorescence emission, thereby allowing us to identify AS-YFP fibrillar deposits due to their very low anisotropy in comparison to the soluble protein.

Additionally, we gained insight into the structural mechanism of AS amyloid assembly from FAIM-based analysis of the aggregation pathway of AS-YFP. Soluble intermediates present during the early stages of the lag phase of aggregation display values of anisotropy lower than monomeric AS-YFP,

indicative of transfer of energy between AS-YFP molecules due to protein oligomerization. Notably, pre-fibrillar intermediates of aggregation show a much higher anisotropy than soluble oligomeric species. A possible explanation for this has its origins in the FRET formalism. Successful energy transfer between two fluorophores depends not only on proximity and spectral overlap but also on the orientation between the transition dipole moments of the FRET pair (termed κ^2).[48,66] Because of its dynamic nature, soluble oligomeric species of AS-YFP would allow the fluorophore to adopt various orientations, increasing the probability of energy transfer and, for this reason, decreasing anisotropy. Conversely, the relatively high anisotropy evidenced in pre-fibrillar aggregates would then arise from the YFP moiety positioned in a restricted subset of orientations, not highly efficient for energy transfer. In amyloid fibrils, the orientation between the fluorophores would continue to be less productive for energy transfer; however, the high fluorophore density of the amyloid state dramatically increases the probability of energy migration, thereby decreasing anisotropy.

From a mechanistic point of view, the low homoFRET in pre-fibrillar aggregates reflects the less compact and disordered architecture of this species in comparison to amyloid fibrils, supported by other biophysical evidence published elsewhere.[17,52] Moreover, the width and irregular shape of the anisotropy histograms corresponding to early pre-fibrillar aggregates are a consequence of the heterogeneous mixture of morphologies previously evidenced for such species.[17,54] Interestingly, our FAIM data on AS-YFP suggest that the maturation from pre-fibrillar aggregates to amyloid fibrils in AS occurs post-insolubilization. The results obtained in these *in vitro* experiments pave the way to further use of FAIM to investigate amyloid formation *in vivo*, exploiting the occurrence of homoFRET.

It is important to note that the use of homoFRET for probing amyloid deposition largely depends on the choice of a fluorophore with intrinsically high anisotropy, such as fluorescent proteins. Hence, tagging amyloidogenic proteins with small organic dyes ($r<0.02$) would not allow straightforward homoFRET-based differentiation of soluble and amyloid fractions. We have demonstrated here, however, that anisotropy measurements could still be used in such cases to follow the increase in size of the protein assembly involved and the enhanced rigidity of the dye, provided that homoFRET is avoided by reducing the fraction of labeled molecules (in our case about to 1%), as recently shown in a high-throughput study.[67]

In conclusion, our results strongly support the use of the AS-YFP protein as a robust and reliable model for AS amyloid aggregation. Moreover, this work demonstrates how the use of fluorescent-protein-based quantitative fluorescence microscopy, and in particular anisotropy-based imaging, is a valuable approach for noninvasive identification and monitoring of the amyloid aggregation of proteins.

Materials and Methods

Expression and purification of proteins

Recombinant expression of AS in the pT7.7 vector and purification to homogeneity followed previously reported protocols.[68] The cDNAs of AS-YFP and BS-YFP gene constructs were amplified from the *C. elegans* expression plasmids pENG001 and pENG002, derived from the pPD30.38 vector, employing PCR with specific primers, and cloned in frame into the vector PET41C (Novagen) employing NdeI-HindIII restriction sites. This vector adds an octarepeat of His residues at the C-terminus of the exogenous gene under the control of the T7 promoter. YFP-containing proteins were expressed in *Escherichia coli* (BL21) and purified by nickel affinity chromatography as follows. The cell pellet was resuspended in buffer A (50 mM Tris–HCl, pH 8.0, and 20 mM imidazole), and the bacterial cells were lysed by sonication on ice (12×15 s pulses, 45 s recovery). Cell debris was spun down by centrifugation (30 m, 22,000*g*), and Ni-NTA resin (equilibrated in lysis buffer) was added to the supernatant and incubated at 4 °C to allow binding. The protein-bound resin was washed three times with buffer B (50 mM Tris–HCl, pH 8, and 50 mM imidazole) for 15 min at 4 °C, followed by centrifugation. The protein was eluted with 500 mM imidazole (in 50 mM Tris–HCl, pH 8). The eluted protein was concentrated using Vivaspin centrifugal devices (10 kDa, Millipore) and then dialyzed against 10 mM Tris–HCl, pH 8. The protein was loaded onto a Superdex S200 column, equilibrated with 25 mM Tris–HCl, pH 7.4, and 100 mM NaCl, allowing isolation of a 95% pure monomeric protein, as judged by SDS-PAGE. The aliquots containing the protein of interest were pooled and concentrated with a Vivaspin centrifugal device. Protein concentration was determined by the absorbance of the protein at 514 nm using an extinction coefficient of 84,000 M^{-1} cm^{-1}. For preparation of ^{15}N-labeled protein, the same protocol was followed, except that LB medium was replaced by M9 minimal medium supplemented with $^{15}NH_4Cl$ (Cambridge Isotope Laboratories). Alexa-488-labeled AS was a kind gift from Dr. N. Cremades, University of Cambridge. Preparation of Alexa-488 AS was achieved by followed standard protocols of cysteine chemistry and instructions from the manufacturer conjugating Alexa Fluor 488 C5 maleimide (Invitrogen) to a Cys-containing mutant of AS (Ala90Cys) following previously reported protocols.[13]

Amyloid formation assays

Aggregation assays for AS, AS-YFP, and BS-YFP were performed in Eppendorf tubes at 37 °C with gentle agitation (220 rpm) in total volumes of 500 μl (100 μM protein, 25 mM Tris–HCl, pH 7.4, 100 mM NaCl, and 0.01% NaN₃). Fifty-microliter aliquots were taken every 24 h for 6 days and subjected to the required procedures. Aggregated protein was separated from soluble protein by centrifugation for 10 min at 13,000*g*. Aggregation assays with mixtures of AS and AS-YFP (1:1, 9:1) were performed under the same conditions. Aggregation assays for studies employing FAIM were performed as above but with 50 μM protein concentration. For the SDS-containing aggregation assays, 200-μl aliquots of protein solution (20 μM protein, 25 mM Tris–HCl, pH 7.4, 100 mM NaCl, 20 μM ThT, 250 μM SDS, and 0.01% NaN₃) were incubated in a 96-well plate, at 37 °C, under constant shaking (300 rpm) in a fluorescence plate reader (Fluostar Optima, BMG). Samples were assayed in triplicate. Images of the aggregated proteins in the Eppendorf tubes were obtained by UV-mediated excitation using a transilluminator.

Fluorescence spectroscopy

All the fluorescence determinations were performed on a Cary-Eclipse Spectrofluorimeter (Varian). Samples for the ThT binding studies were prepared by adding 10 μl of sample into 1 ml of ThT solution (20 μM in phosphate-buffered saline). Samples were measured in quartz cuvettes with an excitation wavelength of 446 nm, and emission spectra were collected from 460 to 600 nm. The fluorescence of YFP in the total, soluble, and aggregated samples was measured in diluted samples to minimize absorption (1/10 dilution, 10 μM maximum protein concentration). Excitation was set to 515 nm, and emission spectra were collected from 520 to 650 nm. Fluorescence anisotropy was measured on the same samples as above but with the inclusion of manual polarizers, set both on the excitation and emission light pathways. The *G* factor for the instrument at the excitation and emission wavelengths was determined before each round of measurements. Excitation was set to 515 nm, and the parallel and perpendicular emissions were collected at 530 nm, for 5 s, and three measurements were averaged.

Absorbance spectroscopy

Determinations of the absorbance spectra of AS-YFP and BS-YFP samples were performed on a Cary 400 spectrophotometer (Varian). Absorption spectra of aggregated samples were corrected for scattering according to Mach and Middaugh.[69]

CR staining

Aggregated AS-YFP (100 μM) was spun down by centrifugation, and the pellet was resuspended in a similar volume of ethanol (100%). Samples for the CR binding studies were prepared by pipetting 10 μl of aggregated AS-YFP sample (in ethanol) on a glass slide. After drying for 2 min, the slide was fixed in acetone for 15 min. Staining was performed according to Puchtler and Sweat.[70] Slides were imaged on an Olympus BX50 microscope to assess CR binding birefringence in polarized light.

SDS-PAGE

Samples from the aggregation assays were centrifuged (10 min, 13,000*g*) to determine the loss of soluble protein, and the supernatant fraction (1/5 dilution) was resolved on SDS-PAGE under reducing conditions, using NuPAGE gels (4–12% gel, Invitrogen). The gels were stained with Coomassie blue and scanned, and the density of the bands was determined with the software ImageJ (National Institutes of Health).

NMR spectroscopy

^1H–^{15}N HSQC experiments were performed on ^{15}N-labeled AS and AS-YFP at various temperatures on a 500-MHz TCI Bruker spectrometer equipped with a triple-resonance cryo-probe. Solvent suppression followed the water flip back scheme of pulses. Sample conditions were 35- to 50-μM samples in 25 mM Tris–HCl, pH 7.4, 100 mM NaCl, and 10% D_2O. Spectra were acquired using Bruker TopSpin 1.3 and analyzed using Sparky (T. D. Goddard

and D. G. Kneller, SPARKY 3, University of California, San Francisco, CA).

Transmission electron microscopy

For TEM analysis of *in vitro* aggregated samples, a 1:10 dilution of the sample in water was made, which was then applied to Formvar/carbon-coated 400-mesh copper grids (Agar Scientific). Samples were stained with 2% (w/v) uranyl acetate. Images were obtained at various magnifications using a Phillips CEM100 transmission electron microscope. Analysis of fibril width and length was performed employing ImageJ (National Institutes of Health).

Fluorescence anisotropy imaging

Fluorescence polarization anisotropy images were acquired with a customized Olympus FV300 confocal microscope. YFP was excited at 503 nm and Alexa-488 was excited at 495 nm, selecting the respective wavelengths with an acousto-optic tunable filter placed in front of a supercontinuum source (SC450 by Fianium). After the acousto-optic tunable filter, the excitation light is linearly polarized and the plane of polarization was rotated with an achromatic half-wave plate in order to maximize the contrast between the two acquisition channels by imaging a mirror. The system operates with an 80/20 beam splitter in place of a dichroic mirror to allow flexible tuning of the light source.[71] The emitted light was collected by a 60× oil objective, filtered by a 515-nm long-pass filter and focused onto a 300-μm pinhole. The light was then reflected outside the scan head by a mirror, split into the two polarization components with a polarizer beam splitter, and acquired by two fiber-coupled photomultiplier tubes. Anisotropy measurements were calibrated by the estimation of the relative transmission (G) of parallel and perpendicular components, using solutions of known anisotropy: 1 μM YFP solution with $r = 0.30$ or soluble 1 μM Alexa-488 AS with $r = 0.00$. Anisotropy was computed according to the following equation:[48]

$$r = \frac{I_{//} - GI_{\perp}}{I_{//} + 2GI_{\perp}} \qquad (1)$$

Image processing and data analysis were carried out with in-house-developed Matlab (Mathworks) toolbox ImFluo†. Briefly, homogeneous images of fluorescent solutions were processed as acquired by applying Eq. (1); images of aggregates were thresholded in order to discriminate the background (soluble species); the average background intensity was estimated by the average values computed over manually selected region of interest, and these values were subtracted from the intensity acquired on the two channels. Typically, between 5 and 10 images were collected for each sample and time point. Data are presented as mean±standard deviation, and two-tailed unpaired *t* tests were performed to confirm the statistical significance of their difference.

Acknowledgements

Supplementary Data

Supplementary data associated with this article can be found, in the online version, at doi:10.1016/j.jmb.2009.10.066

References

1. Spillantini, M. G., Crowther, R. A., Jakes, R., Hasegawa, M. & Goedert, M. (1998). α-Synuclein in filamentous inclusions of Lewy bodies from Parkinson's disease and dementia with Lewy bodies. *Proc. Natl Acad. Sci. USA*, **95**, 6469–6473.
2. Shults, C. W. (2006). Lewy bodies. *Proc. Natl Acad. Sci. USA*, **103**, 1661–1668.
3. Polymeropoulos, M. H., Lavedan, C., Leroy, E., Ide, S. E., Dehejia, A., Dutra, A. *et al.* (1997). Mutation in the α-synuclein gene identified in families with Parkinson's disease. *Science*, **276**, 2045–2047.
4. Kruger, R., Kuhn, W., Muller, T., Woitalla, D., Graeber, M., Kosel, S. *et al.* (1998). Ala30Pro mutation in the gene encoding α-synuclein in Parkinson's disease. *Nat. Genet.* **18**, 106–108.
5. Chartier-Harlin, M. C., Kachergus, J., Roumier, C., Mouroux, V., Douay, X., Lincoln, S. *et al.* (2004). α-Synuclein locus duplication as a cause of familial Parkinson's disease. *Lancet*, **364**, 1167–1169.
6. Zarranz, J. J., Alegre, J., Gomez-Esteban, J. C., Lezcano, E., Ros, R., Ampuero, I. *et al.* (2004). The new mutation, E46K, of α-synuclein causes Parkinson and Lewy body dementia. *Ann. Neurol.* **55**, 164–173.
7. Singleton, A. B., Farrer, M., Johnson, J., Singleton, A., Hague, S., Kachergus, J. *et al.* (2003). α-Synuclein locus triplication causes Parkinson's disease. *Science*, **302**, 841.
8. Chandra, S., Gallardo, G., Fernandez-Chacon, R., Schluter, O. M. & Sudhof, T. C. (2005). α-Synuclein cooperates with CSPα in preventing neurodegeneration. *Cell*, **123**, 383–396.
9. Cabin, D. E., Shimazu, K., Murphy, D., Cole, N. B., Gottschalk, W., McIlwain, K. L. *et al.* (2002). Synaptic vesicle depletion correlates with attenuated synaptic responses to prolonged repetitive stimulation in mice lacking α-synuclein. *J. Neurosci.* **22**, 8797–8807.

† http://www.quantitative-microscopy.org

10. Eliezer, D., Kutluay, E., Bussell, R., Jr. & Browne, G. (2001). Conformational properties of α-synuclein in its free and lipid-associated states. *J. Mol. Biol.* **307**, 1061–1073.

11. Bodner, C. R., Dobson, C. M. & Bax, A. (2009). Multiple tight phospholipid-binding modes of α-synuclein revealed by solution NMR spectroscopy. *J. Mol. Biol.* **390**, 775–790.

12. Dedmon, M. M., Lindorff-Larsen, K., Christodoulou, J., Vendruscolo, M. & Dobson, C. M. (2005). Mapping long-range interactions in α-synuclein using spin-label NMR and ensemble molecular dynamics simulations. *J. Am. Chem. Soc.* **127**, 476–477.

13. Bertoncini, C. W., Jung, Y. S., Fernandez, C. O., Hoyer, W., Griesinger, C., Jovin, T. M. & Zweckstetter, M. (2005). Release of long-range tertiary interactions potentiates aggregation of natively unstructured α-synuclein. *Proc. Natl Acad. Sci. USA*, **102**, 1430–1435.

14. Lee, J. C., Lai, B. T., Kozak, J. J., Gray, H. B. & Winkler, J. R. (2007). α-Synuclein tertiary contact dynamics. *J. Phys. Chem. B*, **111**, 2107–2112.

15. Urie, K. G., Angulo, D., Lee, J. C., Kozak, J. J., Gray, H. B. & Winkler, J. R. (2009). Synchronous vs asynchronous chain motion in α-synuclein contact dynamics. *J. Phys. Chem. B*, **113**, 522–530.

16. Bucciantini, M., Giannoni, E., Chiti, F., Baroni, F., Formigli, L., Zurdo, J. *et al.* (2002). Inherent toxicity of aggregates implies a common mechanism for protein misfolding diseases. *Nature*, **416**, 507–511.

17. Volles, M. J. & Lansbury, P. T. (2003). Zeroing in on the pathogenic form of α-synuclein and its mechanism of neurotoxicity in Parkinson's disease. *Biochemistry*, **42**, 7871–7878.

18. Outeiro, T. F. & Lindquist, S. (2003). Yeast cells provide insight into α-synuclein biology and pathobiology. *Science*, **302**, 1772–1775.

19. Dedmon, M. M., Christodoulou, J., Wilson, M. R. & Dobson, C. M. (2005). Heat shock protein 70 inhibits α-synuclein fibril formation via preferential binding to prefibrillar species. *J. Biol. Chem.* **280**, 14733–14740.

20. Lashuel, H. A., Hartley, D., Petre, B. M., Walz, T. & Lansbury, P. T., Jr. (2002). Neurodegenerative disease: amyloid pores from pathogenic mutations. *Nature*, **418**, 291.

21. Giepmans, B. N., Adams, S. R., Ellisman, M. H. & Tsien, R. Y. (2006). The fluorescent toolbox for assessing protein location and function. *Science*, **312**, 217–224.

22. Outeiro, T. F., Putcha, P., Tetzlaff, J. E., Spoelgen, R., Koker, M., Carvalho, F., Hyman, B. T. & McLean, P. J. (2008). Formation of toxic oligomeric α-synuclein species in living cells. *PLoS ONE*, **3**, e1867.

23. Roberti, M. J., Bertoncini, C. W., Klement, R., Jares-Erijman, E. A. & Jovin, T. M. (2007). Fluorescence imaging of amyloid formation in living cells by a functional, tetracysteine-tagged α-synuclein. *Nat. Methods*, **4**, 345–351.

24. Opazo, F., Krenz, A., Heermann, S., Schulz, J. B. & Falkenburger, B. H. (2008). Accumulation and clearance of α-synuclein aggregates demonstrated by time-lapse imaging. *J. Neurochem.* **106**, 529–540.

25. Roberti, M. J., Morgan, M., Menendez, G., Pietrasanta, L. I., Jovin, T. M. & Jares-Erijman, E. A. (2009). Quantum dots as ultrasensitive nanoactuators and sensors of amyloid aggregation in live cells. *J. Am. Chem. Soc.* **131**, 8102–8107.

26. Betzig, E., Patterson, G. H., Sougrat, R., Lindwasser, O. W., Olenych, S., Bonifacino, J. S. *et al.* (2006). Imaging intracellular fluorescent proteins at nanometer resolution. *Science*, **313**, 1642–1645.

27. van Ham, T. J., Thijssen, K. L., Breitling, R., Hofstra, R. M., Plasterk, R. H. & Nollen, E. A. (2008). *C. elegans* model identifies genetic modifiers of α-synuclein inclusion formation during aging. *PLoS Genet.* **4**, e1000027.

28. Hamamichi, S., Rivas, R. N., Knight, A. L., Cao, S., Caldwell, K. A. & Caldwell, G. A. (2008). Hypothesis-based RNAi screening identifies neuroprotective genes in a Parkinson's disease model. *Proc. Natl Acad. Sci. USA*, **105**, 728–733.

29. Rockenstein, E., Schwach, G., Ingolic, E., Adame, A., Crews, L., Mante, M. *et al.* (2005). Lysosomal pathology associated with α-synuclein accumulation in transgenic models using an eGFP fusion protein. *J. Neurosci. Res.* **80**, 247–259.

30. Muchowski, P. J., Ramsden, R., Nguyen, Q., Arnett, E. E., Greiling, T. M., Anderson, S. K. & Clark, J. I. (2008). Noninvasive measurement of protein aggregation by mutant huntingtin fragments or α-synuclein in the lens. *J. Biol. Chem.* **283**, 6330–6336.

31. Cooper, A. A., Gitler, A. D., Cashikar, A., Haynes, C. M., Hill, K. J., Bhullar, B. *et al.* (2006). α-Synuclein blocks ER-Golgi traffic and Rab1 rescues neuron loss in Parkinson's models. *Science*, **313**, 324–328.

32. Wang, J., Farr, G. W., Hall, D. H., Li, F., Furtak, K., Dreier, L. & Horwich, A. L. (2009). An ALS-linked mutant SOD1 produces a locomotor defect associated with aggregation and synaptic dysfunction when expressed in neurons of *Caenorhabditis elegans*. *PLoS Genet.* **5**, e1000350.

33. Nollen, E. A., Garcia, S. M., van Haaften, G., Kim, S., Chavez, A., Morimoto, R. I. & Plasterk, R. H. (2004). Genome-wide RNA interference screen identifies previously undescribed regulators of polyglutamine aggregation. *Proc. Natl Acad. Sci. USA*, **101**, 6403–6408.

34. Satyal, S. H., Schmidt, E., Kitagawa, K., Sondheimer, N., Lindquist, S., Kramer, J. M. & Morimoto, R. I. (2000). Polyglutamine aggregates alter protein folding homeostasis in *Caenorhabditis elegans*. *Proc. Natl Acad. Sci. USA*, **97**, 5750–5755.

35. Hamada, D., Tsumoto, K., Sawara, M., Tanaka, N., Nakahira, K., Shiraki, K. & Yanagihara, I. (2008). Effect of an amyloidogenic sequence attached to yellow fluorescent protein. *Proteins*, **72**, 811–821.

36. Nagai, T., Ibata, K., Park, E. S., Kubota, M., Mikoshiba, K. & Miyawaki, A. (2002). A variant of yellow fluorescent protein with fast and efficient maturation for cell-biological applications. *Nat. Biotechnol.* **20**, 87–90.

37. Nilsson, M. R. (2004). Techniques to study amyloid fibril formation in vitro. *Methods*, **34**, 151–160.

38. Soper, J. H., Roy, S., Stieber, A., Lee, E., Wilson, R. B., Trojanowski, J. Q. *et al.* (2008). α-Synuclein-induced aggregation of cytoplasmic vesicles in *Saccharomyces cerevisiae*. *Mol. Biol. Cell*, **19**, 1093–1103.

39. Fernandez, C. O., Hoyer, W., Zweckstetter, M., Jares-Erijman, E. A., Subramaniam, V., Griesinger, C. & Jovin, T. M. (2004). NMR of α-synuclein–polyamine complexes elucidates the mechanism and kinetics of induced aggregation. *EMBO J.* **23**, 2039–2046.

40. Croke, R. L., Sallum, C. O., Watson, E., Watt, E. D. & Alexandrescu, A. T. (2008). Hydrogen exchange of monomeric α-synuclein shows unfolded structure persists at physiological temperature and is independent of molecular crowding in *Escherichia coli*. *Protein Sci.* **17**, 1434–1445.

41. Hsu, S. T., Bertoncini, C. W. & Dobson, C. M. (2009). Use of protonless NMR spectroscopy to alleviate the loss of information resulting from exchange-broadening. *J. Am. Chem. Soc.* **131**, 7222–7223.

42. Hsu, S. T., Behrens, C., Cabrita, L. & Dobson, C. M. (2009). ^{1}H, ^{15}N and ^{13}C assignments of yellow fluorescent protein (YFP) Venus. *Biomol. NMR Assign.* **3**, 67–72.

43. Uversky, V. N. & Fink, A. L. (2002). Amino acid determinants of α-synuclein aggregation: putting together pieces of the puzzle. *FEBS Lett.* **522**, 9–13.

44. Rivers, R. C., Kumita, J. R., Tartaglia, G. G., Dedmon, M. M., Pawar, A., Vendruscolo, M. *et al.* (2008). Molecular determinants of the aggregation behavior of α- and β-synuclein. *Protein Sci.* **17**, 887–898.

45. Park, J. Y. & Lansbury, P. T., Jr. (2003). β-Synuclein inhibits formation of α-synuclein protofibrils: a possible therapeutic strategy against Parkinson's disease. *Biochemistry*, **42**, 3696–3700.

46. Hashimoto, M., Rockenstein, E., Mante, M., Mallory, M. & Masliah, E. (2001). β-Synuclein inhibits α-synuclein aggregation: a possible role as an anti-parkinsonian factor. *Neuron*, **32**, 213–223.

47. Johnson, J. M. & Betz, W. J. (2008). The color of lactotroph secretory granules stained with FM1–43 depends on dye concentration. *Biophys. J.* **94**, 3167–3177.

48. Lakowicz, J. R. (2006). *Principles of Fluorescence Spectroscopy*, 3rd edit. Springer, New York.

49. Duysens, L. N. (1956). The flattening of the absorption spectrum of suspensions, as compared to that of solutions. *Biochim. Biophys. Acta*, **19**, 1–12.

50. Runnels, L. W. & Scarlata, S. F. (1995). Theory and application of fluorescence homotransfer to melittin oligomerization. *Biophys. J.* **69**, 1569–1583.

51. Gautier, I., Tramier, M., Durieux, C., Coppey, J., Pansu, R. B., Nicolas, J. C. *et al.* (2001). Homo-FRET microscopy in living cells to measure monomer–dimer transition of GFP-tagged proteins. *Biophys. J.* **80**, 3000–3008.

52. Karpinar, D. P., Balija, M. B., Kugler, S., Opazo, F., Rezaei-Ghaleh, N., Wender, N. *et al.* (2009). Pre-fibrillar α-synuclein variants with impaired β-struc-ture increase neurotoxicity in Parkinson's disease models. *EMBO J.* **28**, 3256–3268.

53. Orte, A., Birkett, N. R., Clarke, R. W., Devlin, G. L., Dobson, C. M. & Klenerman, D. (2008). Direct characterization of amyloidogenic oligomers by sin-gle-molecule fluorescence. *Proc. Natl Acad. Sci. USA*, **105**, 14424–14429.

54. Fink, A. L. (2006). The aggregation and fibrillation of α-synuclein. *Acc. Chem. Res.* **39**, 628–634.

55. Steinbrink, J., Liebert, A., Wabnitz, H., Macdonald, R., Obrig, H., Wunder, A. *et al.* (2008). Towards nonin-vasive molecular fluorescence imaging of the human brain. *Neurodegener. Dis.* **5**, 296–303.

56. Yuste, R. (2005). Fluorescence microscopy today. *Nat. Methods*, **2**, 902–904.

57. Heise, H., Hoyer, W., Becker, S., Andronesi, O. C., Riedel, D. & Baldus, M. (2005). Molecular-level secondary structure, polymorphism, and dynamics of full-length α-synuclein fibrils studied by solid-state NMR. *Proc. Natl Acad. Sci. USA*, **102**, 15871–15876.

58. Chen, M., Margittai, M., Chen, J. & Langen, R. (2007). Investigation of α-synuclein fibril structure by site-directed spin labeling. *J. Biol. Chem.* **282**, 24970–24979.

59. Vilar, M., Chou, H. T., Luhrs, T., Maji, S. K., Riek-Loher, D., Verel, R. *et al.* (2008). The fold of α-synuclein fibrils. *Proc. Natl Acad. Sci. USA*, **105**, 8637–8642.

60. Wurth, C., Guimard, N. K. & Hecht, M. H. (2002). Mutations that reduce aggregation of the Alzheimer's Aβ42 peptide: an unbiased search for the sequence determinants of Aβ amyloidogenesis. *J. Mol. Biol.* **319**, 1279–1290.

61. Mukhopadhyay, S., Nayak, P. K., Udgaonkar, J. B. & Krishnamoorthy, G. (2006). Characterization of the formation of amyloid protofibrils from barstar by mapping residue-specific fluorescence dynamics. *J. Mol. Biol.* **358**, 935–942.

62. Thirunavukkuarasu, S., Jares-Erijman, E. A. & Jovin, T. M. (2008). Multiparametric fluorescence detection of early stages in the amyloid protein aggregation of pyrene-labeled α-synuclein. *J. Mol. Biol.* **378**, 1064–1073.

63. Tramier, M. & Coppey-Moisan, M. (2008). Fluores-cence anisotropy imaging microscopy for homo-FRET in living cells. *Methods Cell Biol.* **85**, 395–414.

64. Blackman, S. M., Piston, D. W. & Beth, A. H. (1998). Oligomeric state of human erythrocyte band 3 measured by fluorescence resonance energy homo-transfer. *Biophys. J.* **75**, 1117–1130.

65. Lidke, D. S., Nagy, P., Barisas, B. G., Heintzmann, R., Post, J. N., Lidke, K. A. *et al.* (2003). Imaging molecular interactions in cells by dynamic and static fluores-cence anisotropy (rFLIM and emFRET). *Biochem. Soc. Trans.* **31**, 1020–1027.

66. Jares-Erijman, E. A. & Jovin, T. M. (2006). Imaging molecular interactions in living cells by FRET micros-copy. *Curr. Opin. Chem. Biol.* **10**, 409–416.

67. Luk, K. C., Hyde, E. G., Trojanowski, J. Q. & Lee, V. M. (2007). Sensitive fluorescence polarization technique for rapid screening of α-synuclein oligomerization/fibrillization inhibitors. *Biochemistry*, **46**, 12522–12529.

68. Hoyer, W., Antony, T., Cherny, D., Heim, G., Jovin, T. M. & Subramaniam, V. (2002). Dependence of α-synuclein aggregate morphology on solution condi-tions. *J. Mol. Biol.* **322**, 383–393.

69. Mach, H. & Middaugh, C. R. (1993). Measuring protein spectra in the presence of light scattering. *BioTechniques*, **15**, 240–242.

70. Puchtler, H. & Sweat, F. (1965). Congo red as a stain for fluorescence microscopy of amyloid. *J. Histochem. Cytochem.* **13**, 693–694.

71. Frank, J. H., Elder, A. D., Swartling, J., Venkitaraman, A. R., Jeyasekharan, A. D. & Kaminski, C. F. (2007). A white light confocal microscope for spectrally resolved multidimensional imaging. *J. Microsc.* **227**, 203–215.